



AIAA 96-2784

**A 1000 Hour Wear Test of the NASA
NSTAR Ion Thruster**

**James E. Polk
Michael J. Patterson
John R. Brophy
Vince K. Rawlin
Jim S. Sovey
Roger M. Myers
John J. Blandino
Keith D. Goodfellow
Charles E. Garner**

**Jet Propulsion Laboratory
Pasadena, CA 91109**

**Lewis Research Center
Cleveland, OH 44135**

**32nd AIAA/ASME/SAE/ASEE
Joint Propulsion Conference and Exhibit
July 1-3, 1996 / Lake Buena Vista, FL**

A 1000 Hour Wear Test of NASA's NSTAR Ion Thruster

J. E. Polk, M. J. Patterson, J. R. Brophy, V. K. Rawlin,
J. S. Sovey, R. M. Myers, J. J. Blandino, K. D. Goodfellow and C. E. Garner

Abstract

In a NASA program to validate 30 cm xenon ion thruster technology for use in planetary missions a combination of analysis and testing is being used to establish engine reliability. Five long duration tests are planned to identify new failure mechanisms and characterize the parameters which drive known damage accumulation failure modes. In the first of these tests a number of severe engine wear and material redeposition processes were observed and the engine design was modified to address these issues. A 1000 hour wear test was then conducted to verify that the design changes successfully reduced the engine wear and material deposition rates. Because of an error in flow rate calibrations the test was conducted at a somewhat lower engine performance level than planned, but the test demonstrated that the erosion processes were virtually eliminated by the design changes. Information on several important failure mechanisms gained from both of these tests is now being incorporated in probabilistic failure models and preparations for an 8000 hour wear test are proceeding.

Introduction

Xenon ion propulsion offers a number of benefits for planetary mission applications. Because of its high efficiency and specific impulse capability, ion propulsion can significantly decrease the propellant mass or deliver more payload mass and, for many planetary missions, substantially decrease the trip time. NASA's 30 cm xenon ion thruster technology is being validated for use in planetary missions in the NASA Solar Electric Propulsion (SEP) Technology Application Readiness (NSTAR) program. This program is

designed to develop the industrial capability to produce flight engine, power processor and propellant feed system hardware and demonstrate that the technology is mature enough for flight applications. This latter portion of the program is focussed largely on providing flight program managers with sufficient information on performance, reliability and spacecraft interactions to give them the confidence to use the technology.

The technology validation involves a large ground test program concentrating on the demonstration of engine performance over the required throttling range, characterization of the engine and plume interactions with the spacecraft, and demonstrating sufficient engine service life capability for demanding planetary missions. Because ion engines are inherently low thrust devices, extremely long burn times are required. For instance, a typical small body rendezvous mission would require an engine life of 1000-1200D¹ hours. Demonstrating engine reliability for such a long service life by testing alone would be prohibitively expensive, so lifetime assessment for engine wearout failure modes must rely to a large extent on analysis based on an understanding of the physics of failure [1]. The NSTAR program involves a combination of ground-based testing and analysis aimed at providing a quantitative assessment of engine reliability for the dominant failure mechanisms. Five long duration tests are planned. The purpose of these wear tests is to identify unexpected failure modes and characterize the parameters which drive known failure mechanisms. In the first test, 2000 hours of operation at the full power point, several potential failure mechanisms were identified and studied in subsequent shorter duration development tests. Design changes resulting from this experience were then validated in a 1000 hour wear test at the full power point, preparatory to starting an endurance test for the full

8000" hour design life. The potential failure mechanisms observed in the 2000 hour test and the engine design modifications are reviewed in the next section. A description of the hardware and the facility used in the 1000" hour test, a summary of engine operation and performance during the test and the results of the Dekst-test engine component analysis are then presented. Finally, the effectiveness of the design modifications in improving engine life, new insights into the failure mechanisms gained from the test and the application of this understanding in the assessment of failure risk is discussed.

Potential Engine Failure Mechanisms Identified in the 2000 Hour Wear Test

The design of the NSTAR ion engine and the initial 2 0 0 0 hour test of the Engineering Model Thruster (EMT) Number 1 are described in detail in Refs. [2,3, 4] and summarized briefly here. The EMT, developed by the Lewis Research Center (LeRC), is a ring-elliptical thruster design based on a functional model thruster which incorporates a number of novel design features aimed primarily at reducing the thruster mass and providing a power throttling envelope of 0.5 to 2.3 kW with design service life of 8000 hours at full power. The thruster consists of a conic discharge chamber which transitions to a short cylindrical section immediately upstream of the ion optics. To minimize thruster mass and simplify fabrication procedures, the discharge chamber is constructed from aluminum and titanium alloys. In the 2000 hour test of EMT1 the interior discharge chamber surfaces were not textured or specially prepared to improve the adhesion of sputter-deposited films.

To simplify the power processing and minimize the number of discharge chamber components subject to sputter erosion the discharge hollow cathode in this initial design did not employ a keeper or starting electrode and discharge coupling to the anode was used for ignition and steady-state operation. The hollow cathode employs a sheathed heater design, derived from the mercury ion thruster, which is used for both activation and ignition of the cathode.

Two grid, molybdenum ion optics derived from an engineering model mercury ion thruster are used on the EMT. The screen electrode is 0.51 mm thick, while the accelerator electrode is 0.38 mm. The screen grid thickness was increased from that on the

functional model thruster to permit reduced accelerator grid operating voltages and increased grid lifetime. The apertures are circular with nominal inner diameters of 1.91 mm and 1.14 mm for the screen and accelerator grids, respectively. The open area fractions are 0.67 and 0.22 and the nominal cold grid gap is set at 0.66 mm. The screen grid was electrically isolated for this test with the expectation that it would float positive of cathode potential, reducing the energy of impinging ions and increasing grid lifetime.

The 2000 hour test was conducted at the full power point. During an interruption of the test after 876 hours of operation severe erosion of the discharge cathode assembly was noted. While the orifice and chamfer appeared to be undamaged, the outer edge of the orifice plate was eroded to the extent that the electron beam weld bead on the periphery was no longer visible. Damage to the heater coil outer sheath on the portion of the first turn facing downstream was also observed. The entire cathode assembly was replaced and the 2000 hour test was completed. Similar erosion was found on the cathode assembly used in the second test segment.

The screen grid also experienced unexpectedly high erosion resulting in a significant reduction in the grid thickness. Combined optical and direct measurements of the grid on axis indicated a thickness reduction of approximately 100 to 10 μm at the minimum thickness location along a line joining two screen holes. The reduction in thickness was due to a combination of a uniform electrode thinning as well as chamfering around the upstream perimeters of the screen grid holes in the center of the grid.

There was also significant deposition and spalling of thin films. The spalling films were confined to the downstream end of the discharge chamber on the titanium anode surface, along the interior lip of the forward magnet retention ring and on parts of the main propellant plenum. This was a major concern because of the possibility of electrical shorts caused by spalled flakes of sputter-deposited material.

All other engine components suffered little or no damage. The three potential failure mechanisms identified by this test led to several design modifications. In development tests performed after the wear test it was found that the screen grid could float several volts negative of cathode potential and that the

floating potential was a strong function of propellant efficiency. A shift in the main flow meter calibration of 7.5 percent was discovered after the test, indicating that the propellant efficiency over some portion of the test may have been substantially higher than planned. Measurements of the double-to-single ion current ratio made after the wear test yielded a value of 0.30 at the higher propellant efficiency, while at the intended operating point the ratio was 0.13. The combination of a screen grid potential negative of cathode common and a higher than expected double ion fraction were identified as the primary reasons for the excessive screen grid wear, and the design was modified to electrically connect the screen grid to cathode common and operate at a propellant efficiency of 0.93.

It was expected that this would also reduce the deposition rate of films in the discharge chamber. In addition, the discharge chamber design was modified to improve sputter containment. This design change included the application of grit-blasted stainless steel mesh to the forward end of the discharge chamber on all titanium and stainless steel surfaces and the use of grit-blasting on all other discharge chamber surfaces to produce surface features with a roughness scale of $1.0 \mu\text{m}$. Previous experience indicated that this was sufficient to control flakes up to $30 \mu\text{m}$ thick [5].

The cathode and heater wear mechanism is not well understood, but is apparently related to a source of high energy ions generated near the cathode orifice. Several design changes were implemented to mitigate cathode and heater erosion based on the available evidence. The weld, which joins the orifice plate to the cathode tube, was relocated to the side of the cathode so that it is shielded from the high energy ion flux by the orifice plate. This design change will clearly extend the life of this critical joint. The cathode heater was also retracted so that the downstream surface is 1.7 mm upstream of the cathode tip. In long duration tests prior to the 2000 hour test the heaters were retracted and experienced 110 erosion, presumably because they were also shielded by the orifice plate. Finally, the cathode assembly has been enclosed within a cylindrical keeper. The gap between the downstream face of the cathode orifice plate and the upstream side of the keeper orifice plate is as small as possible in an attempt to shield the orifice plate from the high energy ions.

The objectives of the 1000 hour test were to demonstrate that these design changes were successful in reducing the component wear rates and sputter deposit flake formation, obtain additional information on these wear processes that could be used to improve the engine reliability assessment and test the facility and operating procedures that would be used for the subsequent 8000 hour wear test.

Description of the Engine and the Endurance Test Facility

The Wear Test Engine

The thruster used in the 2000 hour test was subsequently used in a number of development tests and then retrofitted to incorporate the design modifications. The ion optics installed for the 1000 hour test had been used prior to that for about 200 hours of operation at the full and minimum power levels in a relatively small vacuum facility at LeRC. A new neutralizer assembly and discharge cathode assembly with keeper electrode were installed. This new configuration was then designated EMT1b.

The engine in the wear test configuration was tested at six operating points spanning the throttling range after assembly at LeRC and before delivery to the Jet Propulsion Laboratory (JPL) for the wear test. These tests were repeated at JPL, after delivery to ensure that the engine had not been damaged during transport and to compare the repeatability of measurements between facilities. The discharge voltage measured in JPL's facility was consistently lower than that measured at Lewis and the discharge current correspondingly higher. In preparation for the 8000 hour test after the completion of the 1000 hour test this discrepancy was traced to an error in the flow rate measurements made at JPL. The cause of the measurement error is discussed below and the determination of the true flow rates is described in the Appendix.

Vacuum Facility

The test was performed in a 3 m diameter, 10 m long stainless steel vacuum chamber pumped by three 1.22 m diameter CVI cryopumps with a pumping speed of 45-50 kL/s on xenon and 4 cryopumps consisting of 0.48 m diameter pure aluminum disks mounted on

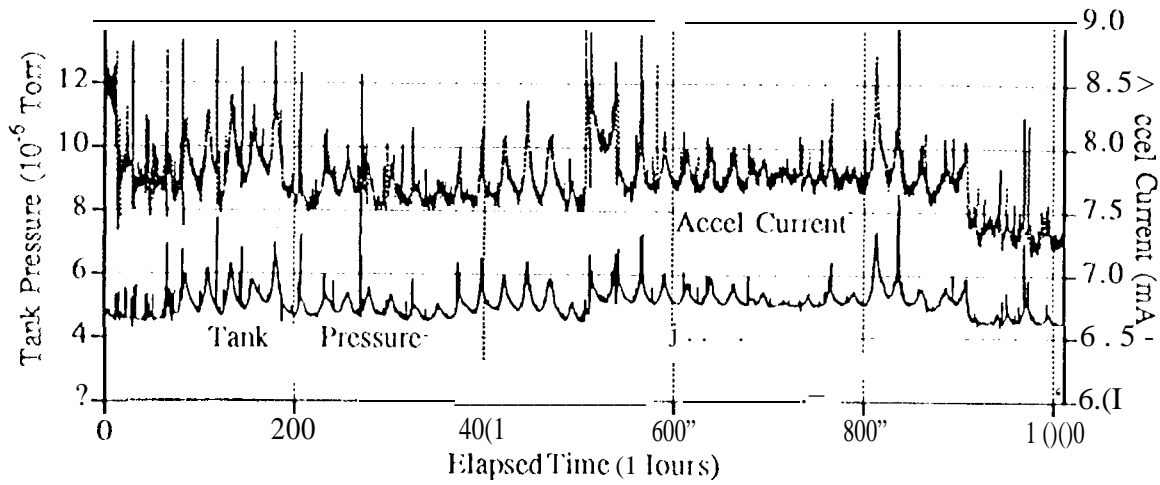


Figure 1: Tank pressure and accelerator grid current during the wear test

Cryomech AL200 coldheads with a pumping speed of about 10 kL/s each, for a total speed of approximately 90 kL/s. The Cryomech He refrigerators were optimized to provide 100 W of cooling capability at 40 K, a temperature sufficiently low to cryopump xenon. The sides of the aluminum plates facing the vacuum chamber walls were covered in multi-layer insulation to reduce the heat load to this surface, so the sides facing inward served as the pumping surfaces. The disks were sized for a theoretical pumping speed of 10 kL/s each with 80 W of heat load at an ambient temperature of 20 degrees C. The measured pumping speed matched the theoretical, but the thermal design was apparently marginal. After about 50 hours of operation small pieces of xenon ice started to fall from the pumping surfaces, causing small pressure spikes several times per day, particularly during the hottest hours. The data acquisition and control system was programmed to turn off the high voltage during these events to avoid engine operation with a high accelerator grid current. The tank pressure as a function of elapsed time with beam extraction is plotted in Fig. (1), which shows that the pressure was typically about 4.5×10^{-6} Torr up to run hour 519, at which point one of the Cryomech pumps failed and the pressure rose to 5×10^{-6} Torr. The facility base pressure was typically 1.2×10^{-7} Torr. When this pump was

repaired at run hour 910, the pressure returned to the previous value. There is also a clear day-night cycle in the tank pressure, which reflects the pumps' sensitivity to the ambient temperature. The development of the 40 K xenon cryopumps is discussed in more detail in [6]. For the 8000" hour test an improved thermal design which increased the pumping speed and appears to have solved the problem with pressure spikes was implemented. This system is also described in this reference.

To reduce the amount of facility material back-sputtered onto the engine, the walls and rear of the chamber were lined with graphite panels, which have a sputter yield about 310 times lower than stainless steel. To further reduce the backscatter rate the panels in the rear of the chamber were arranged in a chevron pattern. Because the sputtered material leaves the surface with a cosine distribution, perhaps with a slightly forward-scattered component, angling the surfaces in such a configuration directs most of the sputtered material away from the engine. The efficacy of this design was demonstrated in a 6000 hour test of the Russian SPT 100 stationary plasma thruster[7] by the low deposition rates on the engine and the large amounts of graphite flakes found behind the chevrons after the test. In the 1000 hour wear test the backscatter rate was monitored with a

quartz crystal microbalance (QCM) mounted next to the engine in the plane of the grids, which indicated a deposition rate of $0.16 \text{ mg/cm}^2 \text{ hr}$ or $0.7 \mu\text{m}/\text{hr}$. Post test analysis of the dense graphite film on the QCM revealed an actual thickness of 0.7 microns, which agreed well with the indicated rate and the thickness of other films collected from the facility.

Propellant Feed System

The propellant feed system was constructed from ultra-high purity components, electropolished stainless steel tubing and welded joints or fittings with metal face seals. The main propellant line was fed from one xenon bottle and the cathode and neutralizer lines were manifolded together and fed from a second cylinder. Each cylinder had a two-stage regulator providing a regulated pressure of about 344 kPa (35 psig). The flow rates were controlled with manual micrometer valves mounted inside the vacuum chamber so that all lines exposed to air had internal xenon pressures above atmospheric. This approach was chosen over conventional flow controllers to minimize the risk of air leaks into the propellant lines. The flow rate in each line was measured with Unit Instruments flow meters. Each line had a bypass around the flow meter, which allowed the flow meters to be isolated with valves located upstream and downstream to monitor the output voltage at zero flow without interrupting flow to the engine. The flowmeter zeroes were checked daily throughout the test and re-zeroed when necessary to prevent flowrate measurement errors associated with zero drift. The Unit Instrument flow meters were found to be extraordinarily stable, requiring adjustment only a few times during the 1000 hours.

The flow could be diverted through two calibration ports so the main and both cathode flow meters could be calibrated in-situ. The flow meters were calibrated using a Teledyne Hastings HB M-1A bubble volumeter. The accuracy of this calibration device has been checked against an NIST-traceable piston prover at the MKS Corporation in Costa Mesa, California with nitrogen over a range of 5 to 100 sccm [8,9], against an NIST-traceable MKS Cali-flow system in JPL's calibration laboratory with argon from 20 to 96 sccm [10] and more recently against an NIST-traceable George K. Porter Vol-U Meter from the Dick Munns Com-

pany in Los Alamitos, California with xenon from 2 to 30 sccm. Each of the three comparisons demonstrated that the bubble volumeter is accurate and repeatable to within 0.8 percent. The bubble volumeter was also compared to piston provers at NIST in Washington, DC with xenon and nitrogen. On the first trip there the NIST representatives measured a xenon flow rate approximately 1 percent lower than JPL's bubble volumeter with what they considered to be their most accurate piston prover at a flow of 60 sccm. On the second trip NIST used another piston prover and obtained flow rates 1.5 to 2.8 percent higher than the bubble volumeter with xenon flows ranging from 17 to 90 sccm. Nitrogen calibrations performed on this trip agreed very well. At the time these results were considered inconclusive; in retrospect the second set of measurements may be consistent with our current understanding of xenon diffusion through the silicone rubber hose used with the bubble volumeter. Three calibrations performed before the start of the test, a calibration done after 650 hours of operation, and two final calibrations after the test showed that the flow meter drift at the flow rates used in the test was less than 1 percent.

As part of the investigation into the difference in discharge voltage and current measurements at JPL and LeRC the flow calibration procedure was reviewed before the start of the wear test. All gas fittings were leak checked and two additional calibrations were performed. When no leaks or apparent problems with the calibration procedure were uncovered, the differences were attributed to different power supplies or other facility-related effects and a decision to begin the test was made. Unfortunately, after the test it was discovered that the 85 cm length of silicone rubber hose used to connect the bubble volumeter to the flow system calibration ports is gas-permeable, even though it has a wall thickness of over 3 mm. The loss of xenon by diffusion through the tube wall resulted in a measured flow rate which was lower than the true flow rate delivered to the engine. The stability of the flow meters and a characterization of the tubing permeability made it possible to accurately correct the flow rates used in the test to their true values, as described in the appendix.

The flow control method used in this test relies on having a well-regulated upstream pressure and a fixed orifice size in the metering valve. Despite tempera-

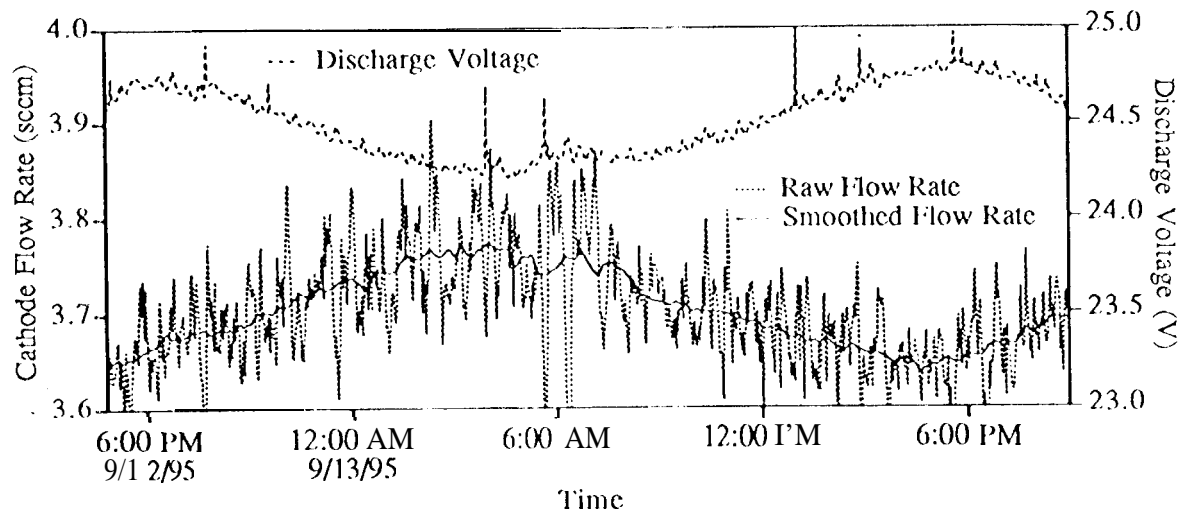


Figure 2: Fluctuations in the indicated cathode flow and the effect on discharge voltage

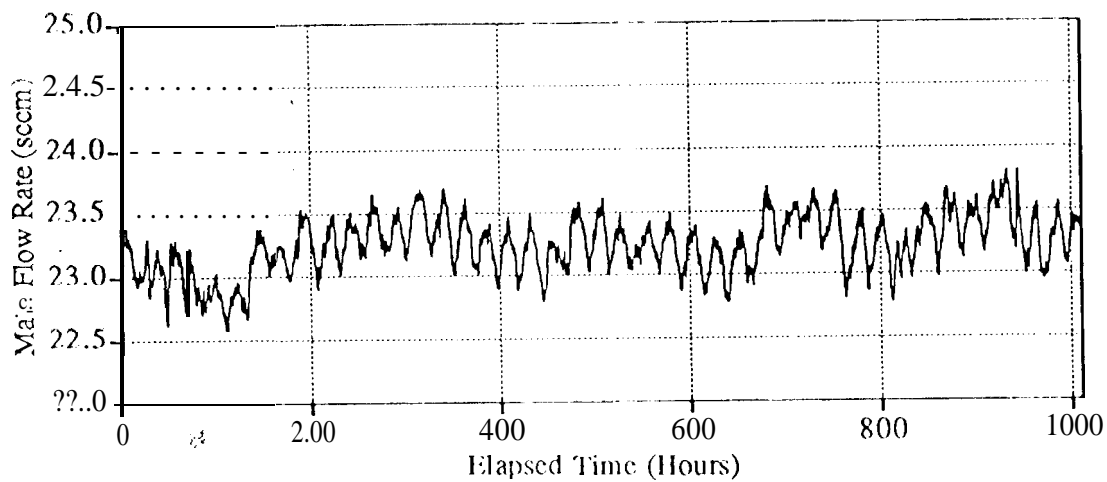


Figure 3: Main flow rate as a function of elapsed time with beam extraction.

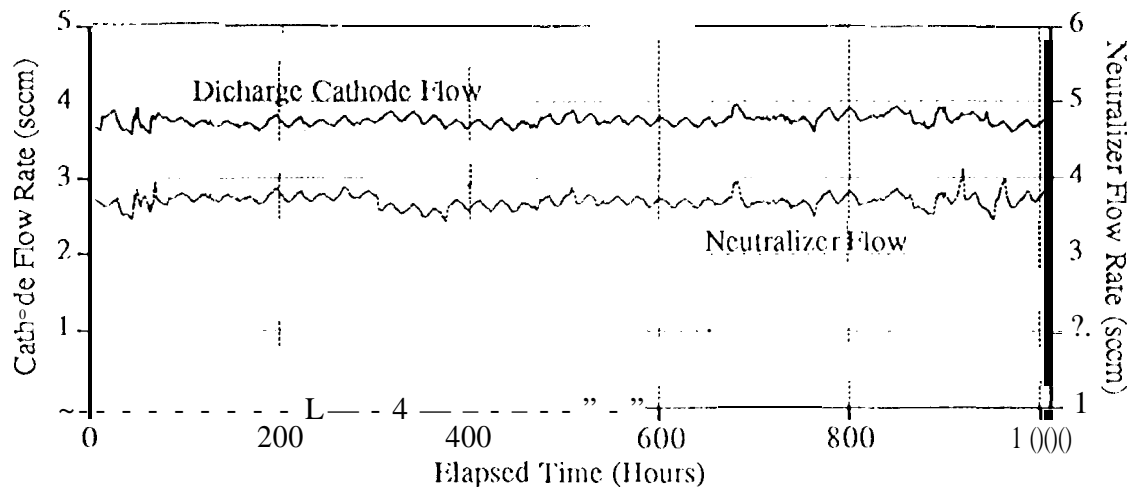


Figure 4: Cathode and neutralizer flow rates

ture control of the regulators and valves to within ± 1 degree C, a diurnal cycle was apparent in each flow rate. Figure (2) shows one period of this day-night cycle in the cathode flow. This effect resulted in a variation in the discharge cathode flow of approximately ± 1.6 percent, a ± 2.5 percent variation in the neutralizer flow and a ± 1.5 percent fluctuation in the main flow. Superimposed on this variation was a higher frequency oscillation with a period of about 20 minutes, evidently caused by regulator hysteresis and the large tubing volumes upstream and downstream of the flow meters. Comparing the flow meter signals with the discharge voltage suggests that the higher frequency fluctuations are not transmitted through the metering valves to the engine, as shown in Fig. (2). While the discharge voltage clearly reflects the 24 hour variation in the cathode flow, the similar amplitude, higher frequency variations do not affect it. The corrected flows with the 20 minute cycle filtered out are shown in Figures (3) and (4) as a function of the elapsed time of operation with beam extraction. The fluctuations in the main flow masked an initial drift downward that was corrected after about 133 hours. The flow oscillations have been eliminated

for the 8000 hour test by shortening the propellant lines and using flow controllers with the solenoid metering valves located in the vacuum chamber in parallel with the manual micrometer valves.

Power Supplies

This test was conducted using commercial power supplies for the beam, accelerator grid, discharge and neutralizer keeper. The discharge cathode keeper electrode was tied to the anode with a $1\text{k}\Omega$ resistor so that it functioned as a start electrode, but did not have a separate power supply. A separate 240 V power supply in parallel with the discharge supply was available to provide a higher DC voltage for ignition, but was not needed in this test. One additional supply was used to heat the neutralizer cathode during conditioning and prior to ignition. The discharge supply was switched to serve as the discharge cathode heater supply during conditioning and before ignition. Neutralizer common was connected to the facility ground with a zener diode to prevent the coupling voltage from exceeding 60 volts. All supplies could be computer-controlled. In this test only the

discharge supply was operated in a closed loop and the discharge current varied to maintain a given beam current. A recycle logic circuit was used to automatically detect and clear grid shorts. If the accelerator or beam supply current exceeded threshold values for more than 50 msec, indicating a short, the high voltage supplies were turned off and the discharge current was reduced to a lower value for approximately 1 second. The high voltage supplies were then ramped up and the discharge current returned to the previous set point. Because of different power supply characteristics, the discharge current had to be reduced to 2 A to successfully recycle the EMT1b. This is lower than the 4 A design point for the NSTAR power processing unit, but only two shutdown events during the test appeared to be caused by discharge extinction during recycles.

Diagnostics

A computer data acquisition and control system was used to monitor facility and engine conditions and control the power supplies. Data were sampled once every 45 seconds, stored on disk once per minute and critical parameters were printed out once every five minutes. The system was programmed to turn off the high voltage supplies or all engine power if out-of-tolerance conditions in certain facility or engine parameters were detected to allow unattended operation. In the event of a computer-initiated shutdown a buffer containing a two minute window of data sampled at 45 second intervals surrounding the event was stored to assist in diagnosing the cause.

Because of the important role double ions appear to have played in the screen grid erosion observed in the 2000 hour test, the double-to-single ion current ratio was monitored throughout this test with an ExB probe mounted in the rear of the chamber. This ion velocity filter uses a static magnetic field crossed with a variable electric field, produced by biasing two electrodes mounted between permanent magnets, to deflect a collimated beam of ions sampled from the plume across a slit in front of a current collector. Because of their differing velocities, the double and single ion currents appear as well-separated peaks when the collector current is plotted as a function of electrode bias voltage. A general description of the probe design can be found in [1-1]. In the unit used in this

test, however, the entrance slit was set at 0.25 mm and the electrodes were biased to equal and opposite voltages so the electric field along the centerline was close to zero. With the smaller entrance slit, the probe sampled ions from a strip 3.1 cm long extending across the entire face of the thruster, so the ratio of measured currents yields an integrated value of the double ion current fraction along the thruster axis.

Faraday probes mounted on arms which could be swung through the beam just downstream of the grids have been used at LeRC and JPL to measure the beam current distribution on EMT1b and EMT2. This distribution controls to some extent the distribution of wear on the accelerator system.

The residual gas content of the facility was monitored with an MKS 111A-100FC residual gas analyzer. This diagnostic demonstrated, for instance, that the pressure spikes consisted almost exclusively of xenon evaporating from ice flakes that had fallen off of the pumps. The tank pressure was monitored with Granville Phillips Stabil Ion Gauges calibrated on both xenon and nitrogen. One gauge was mounted on the side of the chamber and the other inside the chamber behind and above the engine. The gauge mounted on the side of the chamber initially indicated a slightly higher pressure because of water vapor outgassing from the graphite panels. After the panels had been exposed to high vacuum for several days, however, the two gauges agreed well.

Engine Operation and Performance During the Wear Test

The Engine Operating Point for the Wear Test

The wear test was run at the maximum power level of 2.3 kW under the assumption that this operating point subjects the components to the greatest wear. A decision was made prior to the test to operate at a discharge propellant efficiency of 0.93-0.94 to reduce the double ion fraction and provide additional margin on screen grid life. Because of the flow rate calibration error, the actual performance was lower than the target values. The average values of the engine operating and performance parameters are listed in Table (1). The value of the main flow in this table is corrected for ingestion.

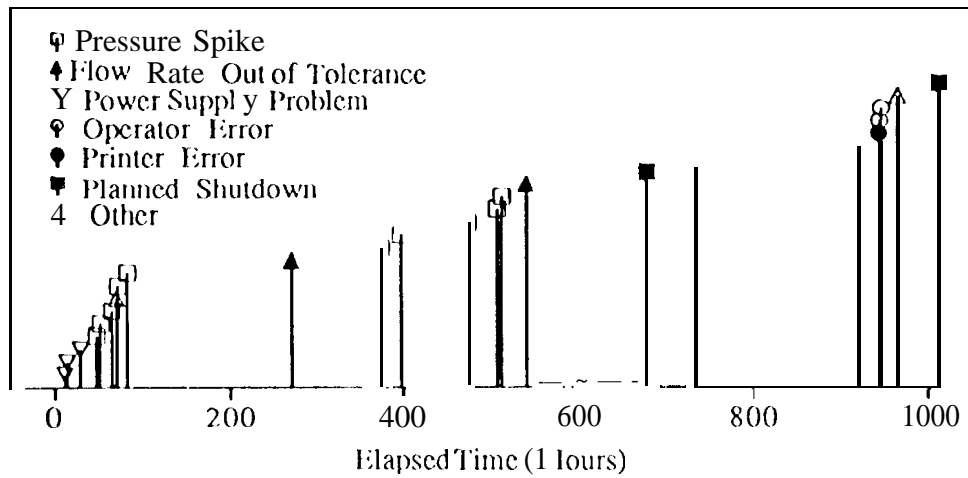


Figure 5: Summary of engine shutdowns.

Test Event History

The wear test was begun immediately after the throttling tests and the choice of an operating point. The history of test interruptions is summarized in Fig. (5). Pressure spikes were the most common cause of engine shutdowns. None of these events required opening the vacuum chamber. After the final shutdown the throttling tests were to be repeated to compare with the initial measurements and a series of tests to measure the sensitivity of the engine performance to small variations in the controllable parameters were planned. An over-current shutdown of the CVI cryopumps due to the failure of a water pump and subsequent damage to the neutralizer by operator error, discussed below, led to a decision not to operate the thruster for these planned measurements. Because the sputter-deposited films on the thruster surfaces had been exposed to nitrogen and water vapor trapped on the cryopumps, further thermal cycling might have caused them to spall and compromised the evaluation of the sputter containment measures.

Discharge Behavior

The discharge cathode was initially started at a target flow rate of 6 sccm (a true flow rate of 6.9 sccm),

and 4.5 A with the full power main flow rate of 23.4 sccm before reducing the cathode flow to the nominal value (3.7 sccm) and throttling to full power. After 187 hours of operation all cathode ignitions were performed at the nominal full power flow rate to match the evolving flight feed system configuration. In all but two cases the discharge ignited on the first application of the discharge supply open circuit voltage of 50 V, and in these two events it started on the second or third attempt with the open circuit voltage. The 240 V start supply was never required to ignite the discharge.

The discharge voltage and current behavior over the 1000 hour test is shown in Fig. (6). Both increase slightly over the first 100 hours, in part because of the downward drift in the main flow rate. It is also likely that direct ion impingement enlarged the accelerator grid hole diameters over this time scale, resulting in greater neutral losses and a higher required discharge power. After the main flow was adjusted at 133 hours elapsed time the discharge voltage and current were approximately constant at 24.2±0.3 V and 13.43±0.09 A, where these and all subsequent variations from the mean run values are expressed as the standard deviation. Variations in the voltage and current are strongly correlated with the diurnal flow rate cycle and longer term flow drift.

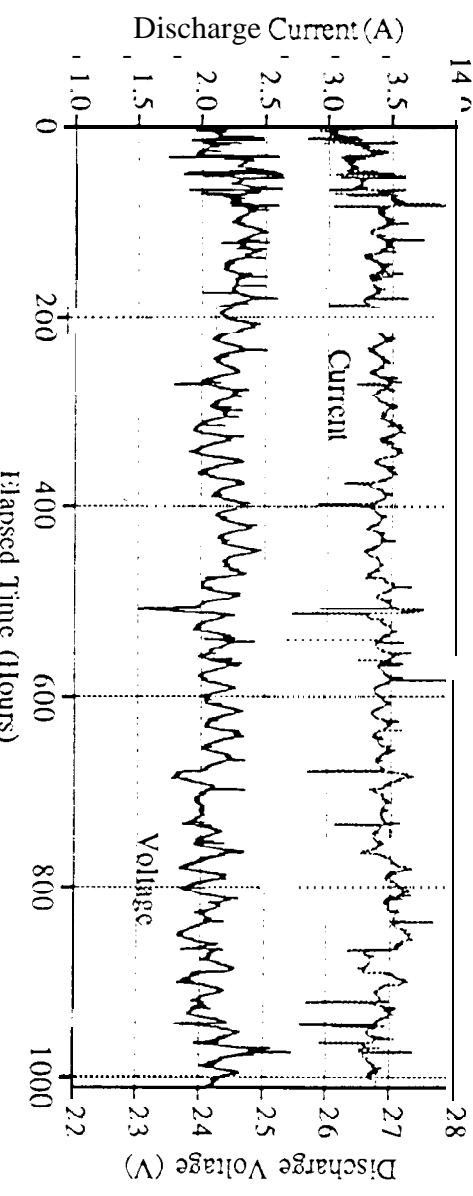


Figure 6: Discharge voltage and current

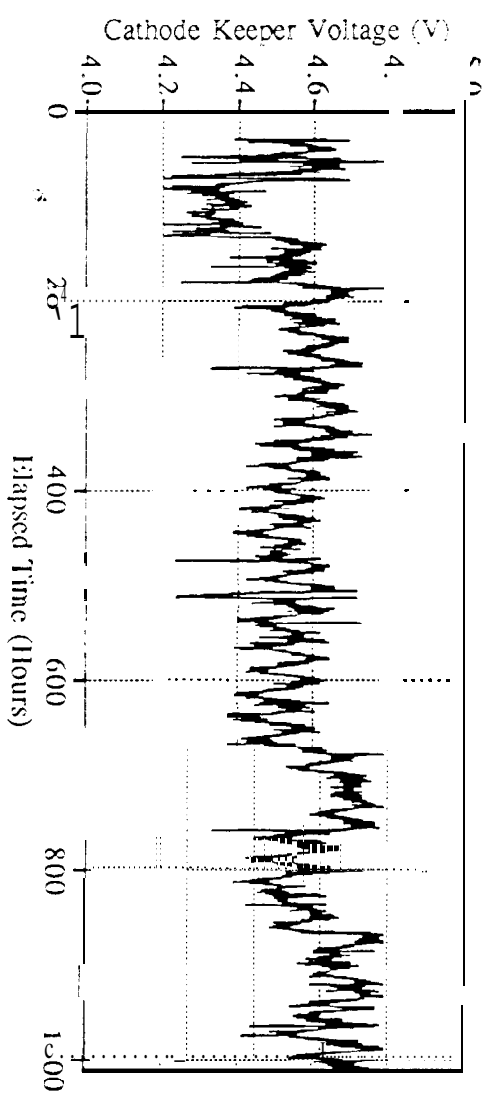


Figure 7: Cathode keeper voltage

Parameter	Average Value
Discharge Current (A)	13.4
Discharge Voltage (V)	24.3
Beam Supply Current (A)	1.770
Beam Supply Voltage (V)	1103
Accelerator Grid Current (mA)	7.76
Accelerator Grid Voltage (V)	-180
Cathode Keeper Voltage (V)	4.6
Neutralizer Keeper Current (A)	1.51
Neutralizer Keeper Voltage (V)	12.97
Coupling Voltage (V)	-13.3
M.sill Flow Rate(ccm)	23.5
Cathode Flow Rate (ccm)	3.75
Neutralizer Flow Rate (ccm)	3.70
Beam Current (A)	1.762
Net Accelerating Voltage (V)	1089
Power (W)	2297
Thrust (mN)	92.9
Specific Impulse (V)	3114
Discharge Propellant Efficiency	0.896
Total Propellant Efficiency	0.789
Efficiency	0.617
Ion Production Cost (eV/ion)	185
Double-to Single Ion Current Ratio	.147

Table 1: Average values of engine operating and performance values in the 1000 hour test.

The cathode keeper voltage, plotted in Fig. (7), was also approximately constant at 4.6 ± 0.1 V with respect to the cathode. The keeper electrode was therefore drawing about 20 mA of current through the $1\text{ k}\Omega$ resistor. The keeper voltage shows the day-night cycle and is correlated with longer term fluctuations in the main flow rate, but is surprisingly insensitive to long period cathode flow variations.

The ion production cost variation over the course of the test, shown in Fig. (8), increases in the first 100 hours from 179 eV/ion to 188 eV/ion, following the increase in discharge current and voltage. It stabilized at a value of 185 ± 1 eV/ion with fluctuations which follow variations in the flow rates, increasing as the flow rate decreases.

Figure (9) displays the distribution of the ion current density in the beam measured near the exit plane and indicates that the plasma density in the discharge chamber is strongly peaked on the centerline. This may be due to operation with no baffle in front of the discharge cathode.

Ion Optics Behavior

The net ion accelerating voltage in the test was 1090.14 V, and the beam current was maintained at 1.762 ± 0.004 A by varying the discharge current, as shown in Fig. (10). The beam current excursions below the setpoint are associated with engine ignitions and those above the setpoint with recycle events. The accelerator grid voltage was set at -1803 1V. The accelerator grid impingement current dropped from an initial value of 8.6 mA to about 7.8 mA in the first 50 hours and thereafter followed variations in the tank pressure, as shown in Fig. (1). The average impingement current value was 7.7 mA, which yields an average ratio of impingement current to beam current of 0.44 percent.

The cumulative number of high voltage arcs as a function of elapsed time with beam extraction is plotted in Fig. (11). The high initial rate is associated with tuning the recycle circuit; the true arc rate at the beginning of the test was about 9 per hour and decreased steadily to 0.5 per hour by the end of the test. The unusually high recycle rate was apparently due to spalling of thin metal films sputter-deposited on the grids during the 200 hour test at low power, which was conducted in a relatively small stainless

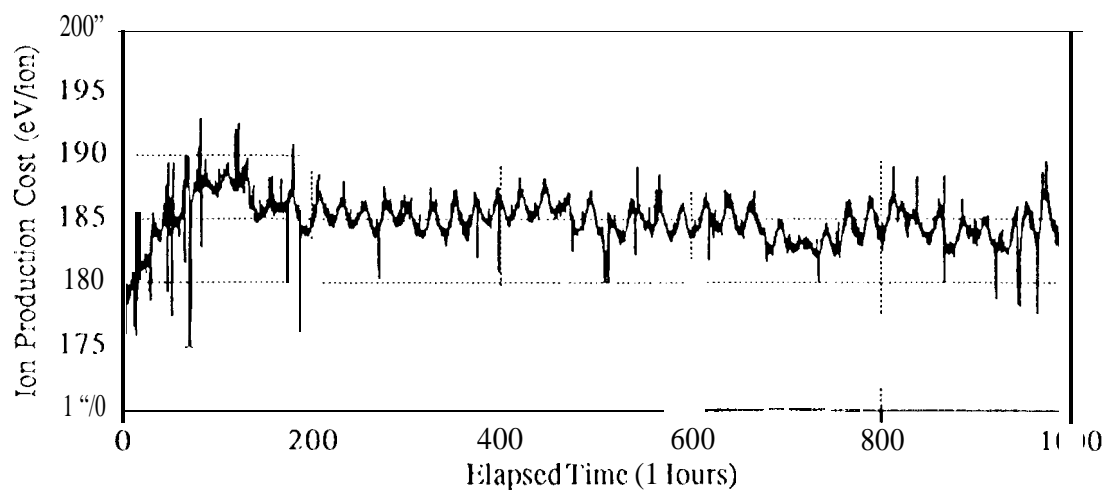


Figure 8: Behavior of the ion production cost during the wear test.

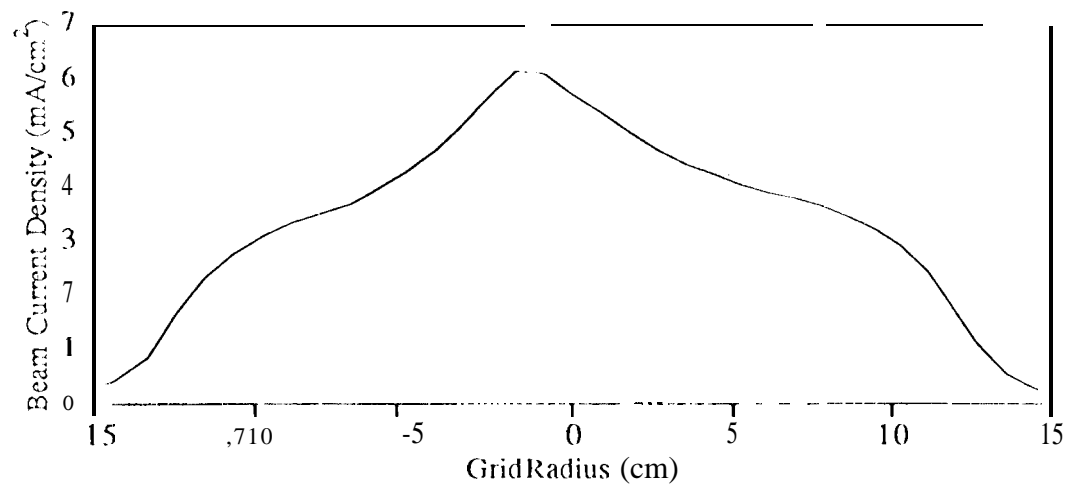


Figure 9: Beam current density profile at the full power point.

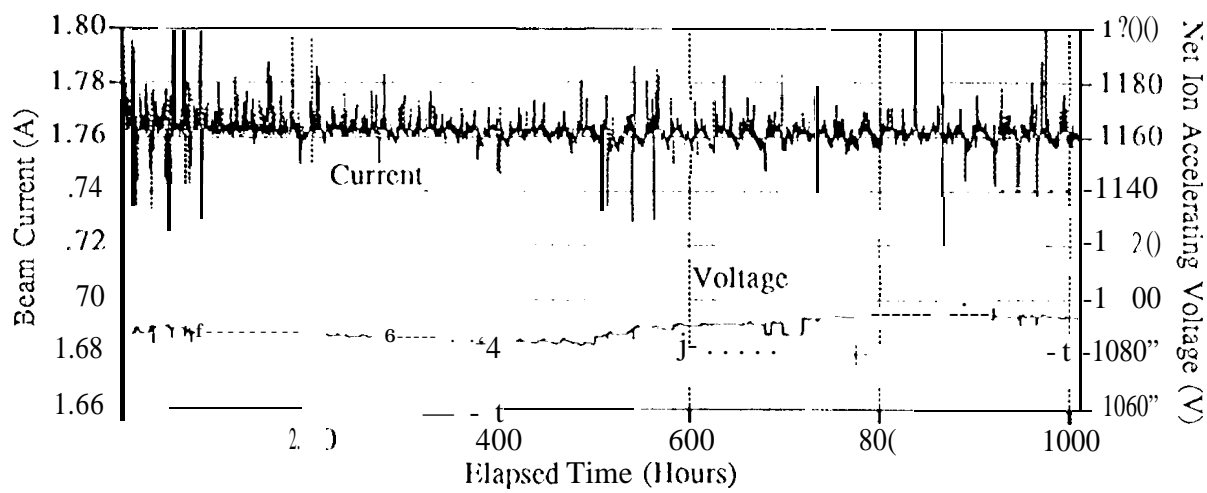


Figure 10: Net ion accelerating voltage and beam current

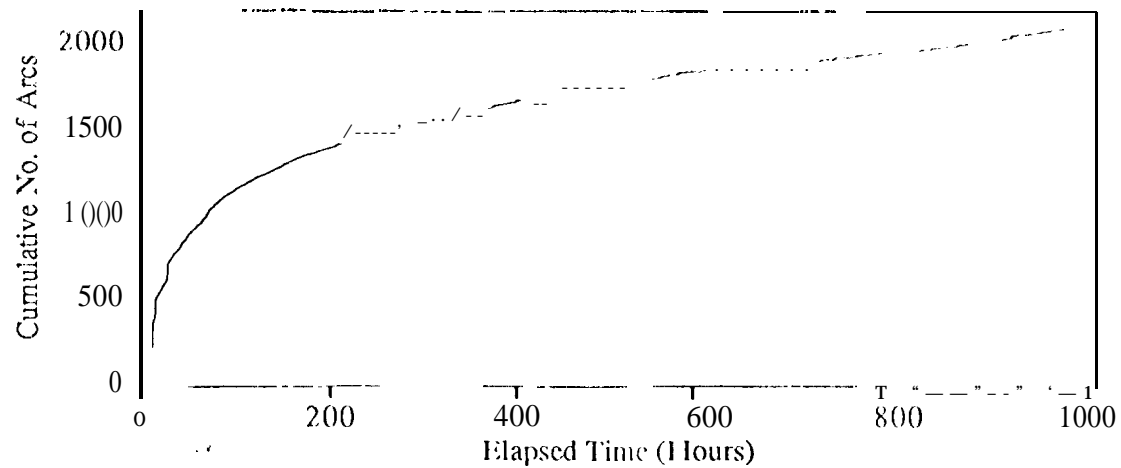


Figure I 1: Cumulative number of high voltage recycles.

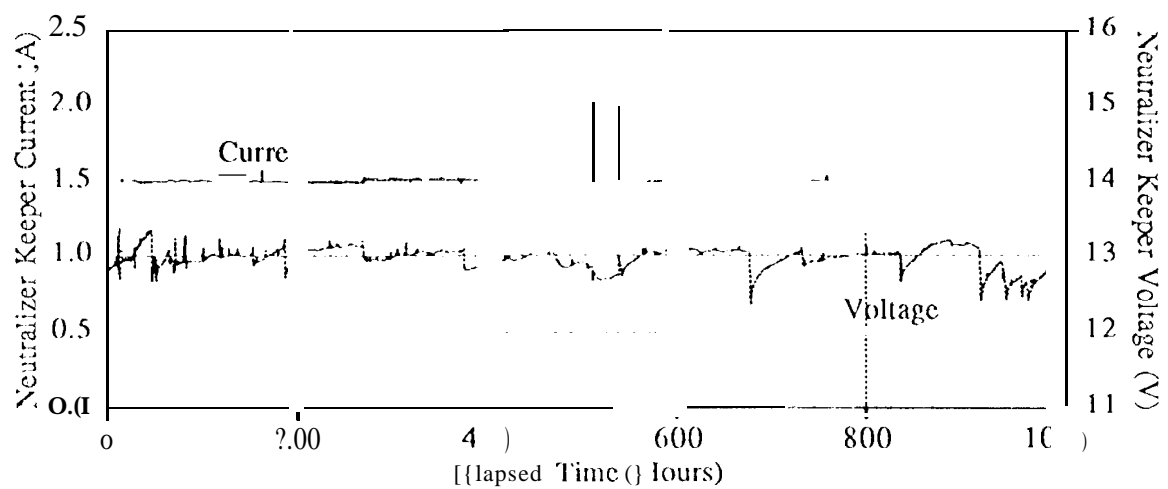


Figure 12: Neutralizer keeper voltage and current

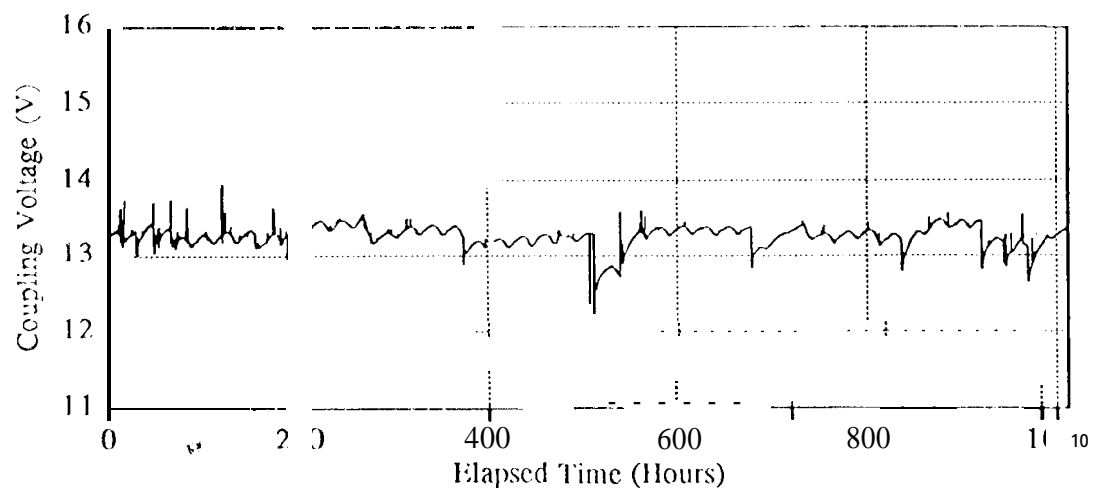


Figure 13: Coupling voltage behavior.

steel chamber. After exposure to air and moisture these thin films are more likely to span, generating shorts between the griebs or sharp points where arcs are likely to initiate. Experience from the first segment of the 2000 hour test and recent testing of EMT2 in the 8000 hour wear test show that extremely low recycle rates are achievable with clean grids or grids with thin film deposits that have not been exposed to air or water vapor.

Neutralizer Operation

The neutralizer cathode was also started at a target flow rate of 6 sccm in the first 187 hours of the test, and then subsequently at the nominal full power flow rate. During the wear test the neutralizer never failed to ignite on the neutralizer keeper supply open circuit voltage of 40 V, and often started at 14-18 V. The neutralizer keeper current and voltage exhibited large amplitude oscillations on startup and the keeper electrode glowed a bright orange. The voltage oscillations would drop from 5-10 V peak-to-peak to about 1 V peak-to-peak and the electrode heating would decrease after several minutes. This transition could be accelerated by the application of heater current for several minutes after ignition, increasing the keeper current to 2 A briefly or turning on the high voltage to increase the cathode emission current. The DC values of the neutralizer keeper voltage and current are shown in Fig. (12). The keeper current was maintained at 1.5 A throughout the test except for one 28 hour period when the current was inadvertently left at 2.0 A after startup. The keeper voltage exhibits long transients after thruster ignition, as in the 2000 hour test, and the steady state voltage achieved after a particular ignition often varies by several tenths of a volt. The mean voltage was 13.0 ± 0.1 V, and it was remarkably insensitive to the neutralizer flow rate variations and the change in keeper current at 512 hours. The coupling voltage, displayed in Fig. (13), also shows transients associated with thruster ignitions and shifting steady state values, but is apparently more sensitive to the keeper current and the tank pressure. It was still relatively stable at 13.3 ± 0.1 V.

After the planned shutdown of the wear test an attempt was made to start the neutralizer prior to repeating the throttling tests. When the neutral-

izer failed to ignite on the power supply open circuit voltage it was discovered that the CVI pumps had shut off and that the true tank pressure was about 1×10^{-4} Torr. This condition was not prevented by the data system monitoring and automatic shutdown algorithm because it was designed only for steady state operation, not for use during ignition. The system has been modified so that hardware and redundant software interlocks disable the power supplies any time the tank pressure exceeds a given setpoint to prevent similar mishaps in the 8000 hour test. Because the Cryomech pumps were still sufficiently cold to trap xenon and water vapor, the ambient gas must have consisted primarily of nitrogen and oxygen. The cathodes were reconditioned and the neutralizer ignited after 12 minutes of heating with the keeper supply open circuit voltage applied. The difficulty in starting and a shift in the voltage-current characteristics as a function of flow rate suggested that the neutralizer operation had changed slightly as a result of heating at the higher tank pressure. This occurred despite a continuous purge of xenon during the tank pressure excursion.

Engine Performance

The engine power consumption with fixed beam current did not vary significantly from the nominal 2.3 kW, as shown in Fig. (14). The variations reflect changes in the discharge power as the discharge current was varied to maintain the desired beam current. If cause the beam current and voltage were controlled, the thrust was constant at 92.9 mN, calculated using the method outlined in [3]. The specific impulse and efficiency, plotted in Fig. (15), varied with changes in the flow rates, but showed no significant decay in performance from the average values of 3114 s and 0.617 over the course of the test.

Figure (16) displays the discharge propellant efficiency as a function of time. Because the beam current was fixed, the propellant efficiency varies only with the flow rates. The ratio of double-to-single ion current measured with the E x B probe is also plotted in this figure and mirrors the discharge propellant efficiency behavior. As the propellant efficiency increases the neutral density in the discharge chamber drops and the electron temperature rises, generating more double ions. The total propellant efficiency, of

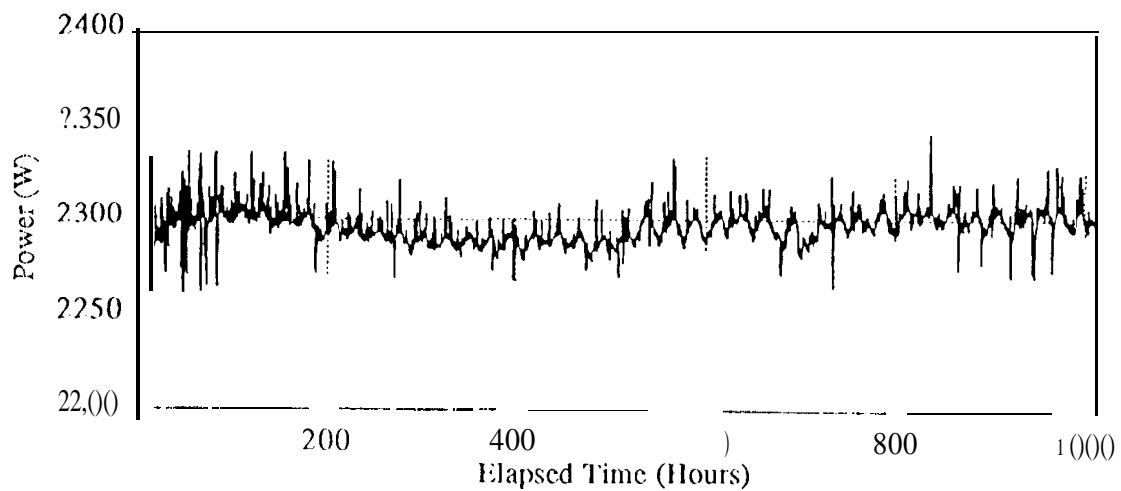


Figure 14: Engine power consumption

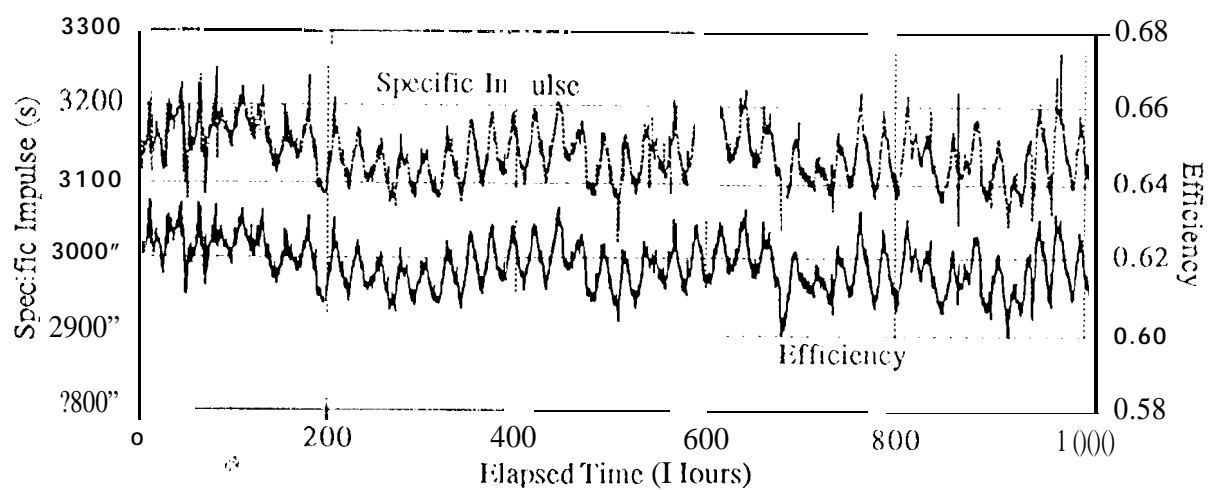


Figure 5: Engine performance during wear test

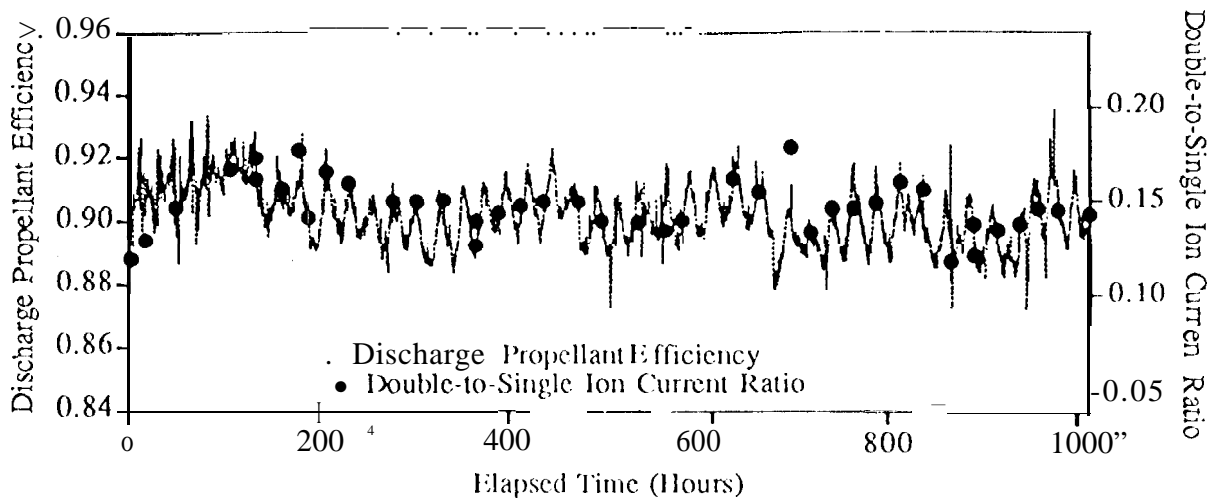


Figure 16: Discharge propellant efficiency and ratio of double-to-single ion currents.

course, shows the same trends with a mean value of 0.789.

Characterization of Engine Wear and Material Deposition

After the endurance test the engine was disassembled and the components subjected to detailed analyses that included mass loss measurements, measurements of dimensional changes and materials analysis

Optics

In general the ion optics suffered very little damage. The accelerator grid was subject to mass loss by direct and charge exchange ion sputtering and deposition of backscattered material from the facility. The net mass change was 2.903 g. A conservative calculation of the amount of carbon sputtered from the graphite panels onto the accelerator grid yields 0.06 g, so the total mass loss did not exceed 2.96 g.

The accelerator grid hole diameters were measured with precision pins in increments of $25 \pm 2.5 \mu\text{m}$ before and after the test. The results are plotted as a function of radius on the grid in Fig. (17) and the net change in the diameters in Fig. (18). The minimum diameter, located at the cusps left by the chemical etching process, was nominally 1.12 mm and increased by as much as $75\text{--}100 \mu\text{m}$ in the center of

the grid over the course of the test. One aperture near the center was notched on one side. Post-test examination revealed a long, narrow metallic deposit on the wall protruding into the corresponding screen grid aperture. This evidently deflected the beamlet into the webbing. Slight notching was also observed in some of the holes at the hole pattern periphery.

The downstream face of the accelerator grid was worn in the characteristic pits and grooves pattern, which is visible in Fig. (19). Optical depth measurements of the maximum eroded depth in the pits between three adjacent holes and the minimum eroded depth in the bridges between two holes were obtained by varying the focus on a microscope. The pit and bridge depths are plotted as a function of radius in Figures (20) and (21). Although no wear in the bridge region was visible before the 1000 hour test, pits with a depth of $13 \pm 5 \mu\text{m}$ had formed in the center of the grid from the 200 hour low power test at relatively high tank pressures.

Two distinct regions of carbon deposits backscattered from the graphite panels were found on the downstream face of the accelerator grid, in a band about 3 cm wide at the periphery the webbing was completely covered with carbon. In the post-test examination after exposure to air regions where the fragile deposits were beginning to spall were observed. Films removed from this region with Kapton tape

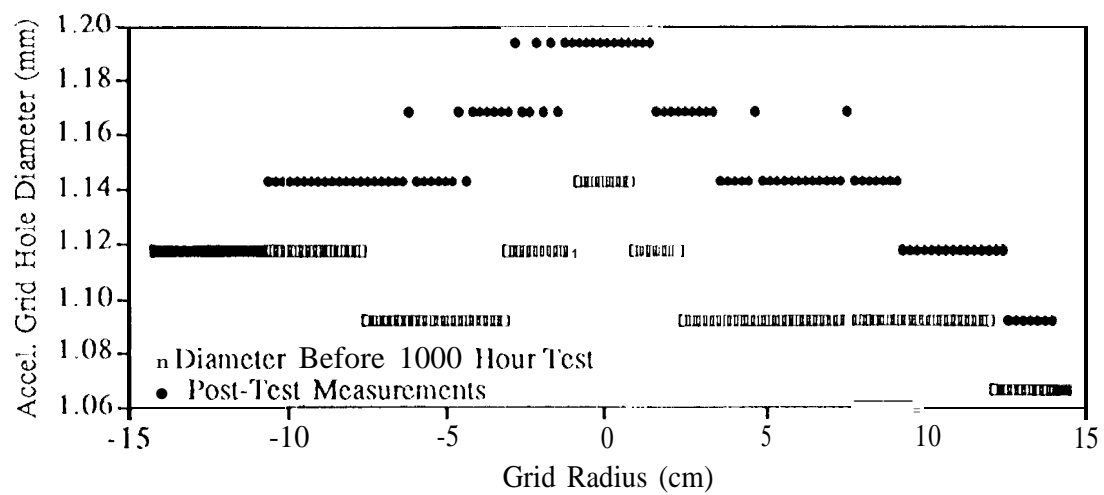


Figure 17: Measurements of accelerator grid aperture diameters.

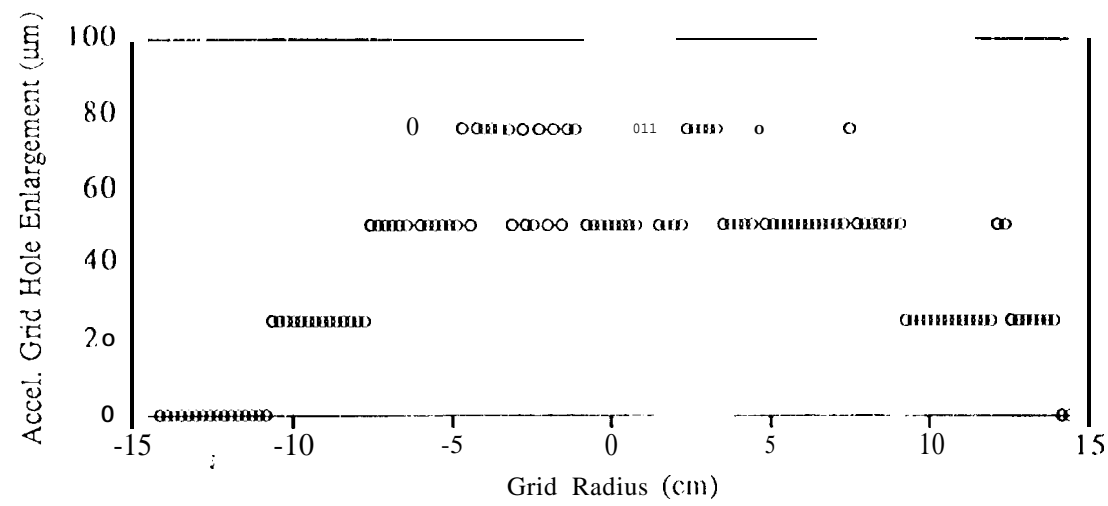


Figure 8: Change in accelerator grid aperture diameters

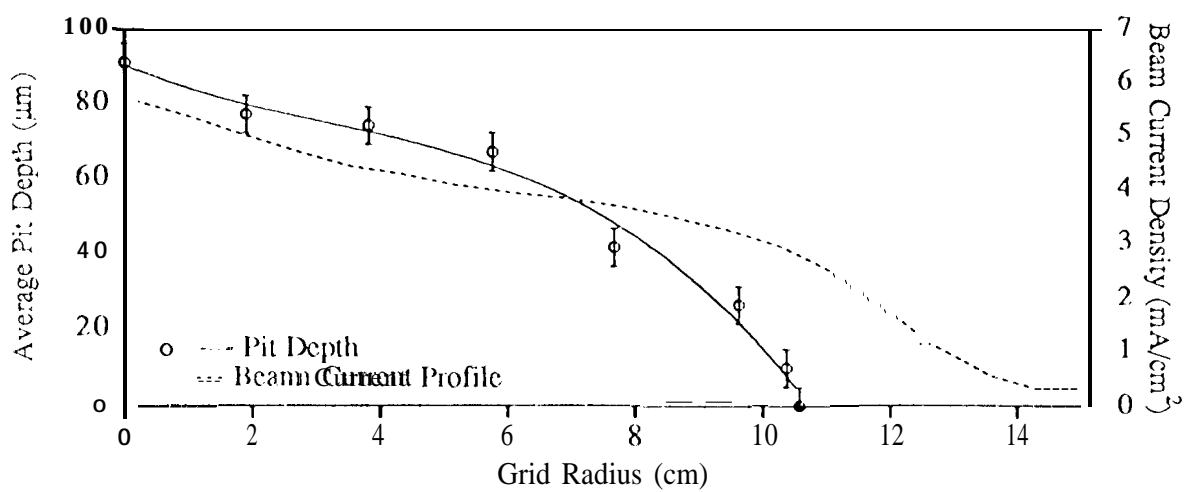


Figure 20: Radial distribution of pit depths

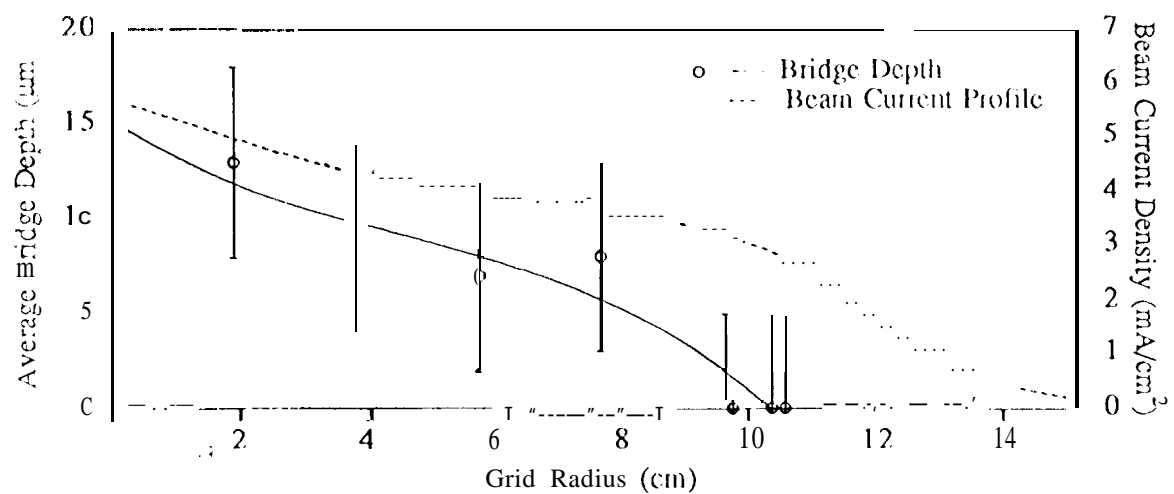


Figure 21: Radial distribution of bridge depths

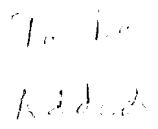


Figure 19 : Erosion and deposition patterns on the downstream face of the accelerator grid.

were examined in a scanning electron microscope (SEM). Elemental analysis indicated almost pure carbon, but the deposits on the grid had a much more porous, grainy appearance compared to the dense carbon films found on the QCM. The deposits had a thickness ranging from 1.3 to $1.8 \mu\text{m}$, which is also thicker than the films on the QCM, but it is unlikely that the fluxes to the grid were substantially higher. Perhaps the higher temperature of the grid or simultaneous ion bombardment leads to the formation of thicker, less dense films.

Inside a radius of 11.6 cm the carbon deposits are confined to the mesas surrounding the holes, as shown in Fig. (19). A very interesting fine structure is apparent in the deposition distribution. The scalloped pattern, which has not been reported previously, shows ion sputter-cleaning, or net erosion, in the pits and grooves. The trenches connecting pits are broadened in the center on lines between two holes. In addition, clean regions on the mesas on lines connecting the hole center to surrounding pits are visible. The asymmetry in the pattern surrounding the holes is probably an indication of a slight misalignment between the two grids, which offsets the beamlets from the accelerator grid hole centers somewhat. The long, shallow patterns visible in this photograph

are etch marks left by the chemical etch process in areas where the photoresist had cracked.

The screen grid had a net $\text{III}_{\text{s,ss}}$ gain of 0.593 g from deposits on the downstream face of the webbing and the cusps in the apertures consisting of molybdenum, presumably eroded from the walls and upstream edges of the accelerator grid holes. Post-test examination of these films in and SEM revealed two distinct layers, of $\approx 1.8 \mu\text{m}$ thick from the 200 hour test at low power and a $2.4 \mu\text{m}$ film on top from the 1000 hour test. There was some evidence of spalling, and it is likely that these films were responsible for the high recycle rate. Very little wear was visible on the upstream face; a change in thickness of only $6 \pm 5 \mu\text{m}$ was measured optically.

Discharge Cathode

The cathode keeper was removed after the test and it and the cathode assembly were inspected and a number of measurements performed. The measurements suggest a change of $25.75 \mu\text{m}$ (1-3 mils) in the keeper orifice plate thickness, but there was no measurable erosion on any other parts of the keeper.

The cathode orifice plate was textured with features $4-14 \mu\text{m}$ high in areas exposed to the discharge plasma through the keeper orifice, but machine marks were still visible on parts of the edges covered by the keeper. Aside from this superficial texturing, there was no evidence of any wear on the cathode orifice plate. The orifice was backlit and photographed at a magnification of 41X and the upstream surface was examined with a boroscope, but there was no evidence of tungsten deposits.

The surface of the tantalum sheath on the heater coil was textured with surface structures with dimensions ranging from $1-10 \mu\text{m}$. This surface roughness is typical of new heaters, and the untextured surface of the TIG weld at the downstream end of the heater confirms that this texturing is not due to ion bombardment in the test. The outer tantalum radiation shield surrounding the cathode/heater showed no evidence of ion bombardment damage when viewed in an SEM capable of resolving erosion features as small as $2 \mu\text{m}$.

Discharge Chamber

No large flakes of material were found in the discharge chamber when the grids were removed after the test and there was no evidence of spalling. Samples were cut from the walls of the discharge chamber in five different locations and sent to the Nonmetallic Materials Division at the University of Dayton Research Institute for analysis. The chemical composition of the coatings was determined using Auger electron spectroscopy and the thickness estimated from Auger depth profiling and electron range calculations in energy-dispersive analysis using X-rays (EDAX). The films consisted of 28 atomic percent molybdenum, 29 percent carbon, 27 percent oxygen, 14 percent nitrogen and 2 percent iron; a mixture of materials likely sputtered from the grids and backscattered from the test facility walls. The maximum coating thickness was estimated to be 1.5 μm with an uncertainty of about 20 percent.

In general the fabrication techniques for installing the sputter-containment mesh seemed to work well, although in some locations near the downstream edge individual spot welds on the mesh had become 100SC, producing small gaps. Samples of the mesh were examined in the SEM, which showed finely textured 11 μm sputter-deposited films that seemed to adhere very well to the grit-blasted surface.

Neutralizer

The neutralizer cathode and keeper were also disassembled and examined. There were no measurable changes in the component dimensions, although sputter-cleaning of part of the downstream keeper surface exposed to divergent beam ions was visible. An 18 μm wide by 58 μm long deposit was found on the upstream surface of the neutralizer cathode orifice plate. Such deposits generally occur when the insert has been exposed to oxygen, which in this case likely happened during the attempt to start the neutralizer with a high residual gas partial pressure at the end of the test. It is probably not indicative of problems associated with operating the cathode at nominal conditions.

Conclusions and Discussion

Effectiveness of the Design Modifications

This test demonstrated that rates of all the life-limiting engine wear and material deposition processes identified in the 2000 hour test have been dramatically reduced. Electrically connecting the screen grid to cathode common reduced its voltage relative to anode potential from 33.0/33.7 V to 24.3 V and the double-to-single ion current ratio was reduced from 30 percent in the conditions at the end of the 2000" hour test to about 15 percent by changing the operating point. These two design changes resulted in a reduction in the maximum screen grid wear rate at the center of the grid from about 46 $\mu\text{m}/\text{khr}$ to about 6. A deterministic calculation based on a linear extrapolation of these wear rates yields an increase in screen grid life from 7,800 hours to about 60,000 hours, where end-of-life is defined as complete wear through in the center of the grid.

These modifications also significantly decreased the risk of flake formation in the discharge chamber by virtually eliminating one of the main sources of deposited material. Film thicknesses measured after the 2000 hour test suggested deposition rates of 2.3–4.0 $\mu\text{m}/\text{khr}$, while the highest rate measured in the 1000 hour test was 1.5 $\mu\text{m}/\text{khr}$. Film adhesion to the sputter-containment mesh was shown to be quite good in this test, and in other experiments such surface preparations have successfully demonstrated containment of up to 30 μm thick films [5]. A deterministic estimate based on this experience yields a service life of up to 20,000 hours before large flakes start to form in the discharge chamber.

The severe cathode orifice plate and heater erosion observed in the previous test was completely eliminated in this test. Changes in orifice plate thickness of 280–290 $\mu\text{m}/\text{khr}$ and complete penetration of the tantalum sheath on both cathode heaters were observed in the 2000 hour test, while no damage to either component was detectable after the 1000 hour test. The major design modification was the addition of the cathode keeper, but the higher flow rate in the 1000" hour test may also have played a role, as discussed below. The engine performance was lower than expected because of the flow rate error, but the test did successfully demonstrate that the engine design should be capable of a very long service life with

minimal risk of failure from these modes.

Understanding of the Failure Mechanisms and Specification of Drivers

In addition to the immediate need to validate design changes before proceeding with a test for the full 8000 hour design life, this wear test provided valuable information on the processes which drive potential failure modes. In some cases these long duration tests have answered certain questions about the behavior of these critical drivers; in other cases they have posed new questions that are defining subsequent tests.

Accelerator Grid Erosion

Although accelerator grid failure by charge exchange ion erosion was not identified as a major problem in the 2000 hour test it may be life-limiting for demanding missions. The accelerator grid erosion observed in this test is not inconsistent with a linear correlation which relates the bridge erosion depth to the sputter yield at normal incidence for an energy corresponding to the grid voltage, the impingement current and the operating time [4]. This correlation does not explicitly account for the detailed spatial distribution of mass loss from the grid which may lead to nonlinear behavior over long periods of operation [12]. This test was too short, however, to discriminate between the predictions of different models. A model which attempts to account for the geometry of mass loss was developed in [13] and incorporated in a probabilistic framework in [14]. This approach yields the probability of engine failure due to grid structural failure as a function of operating time, given the intrinsic variability or uncertainty in the input parameters. Information on the value of these drivers and their variability gained from this test is reviewed here.

The total mass loss from the accelerator grid should scale with the sputter yield, the impingement current and the run time. Estimates of the total mass loss given these values and assuming normally incident ions, however, are typically about two times higher than the measured mass loss [14]. This suggests that the effective sputter yield is lower than that at normal incidence, perhaps because the ions do not strike the surface with an energy corresponding to the full grid potential or because of redeposition of sputtered

material in the erosion pattern. The effective sputter yield was conservatively set equal to that at normal incidence in initial calculations [14], but tests such as

these provide values that can be used to more accurately bound this driver. Using an ion energy of 197 eV, which corresponds to the sum of the grid voltage, the coupling voltage and 4 volts above ground for the beam centerline potential (based on recent measurements with HMT2 in preparation for the 8000 hour test), the measured nucan impingement current and published sputter yield data [15] yields a predicted mass loss of 7.8 g, so the measured mass loss implies an effective sputter yield which is 38 percent of the predicted value. This is to be compared with a value of 17 percent based on a similar calculation for the 2000 hour test. This large difference may simply be due to intrinsic variability or to the different operating conditions. The 2000 hour test was performed at a lower facility pressure and a higher propellant efficiency. Perhaps the impingement current under these conditions is dominated by charge exchange in the neutral gas loss from the engine. These charge exchange collisions might occur much closer to the grids than interactions with residual xenon at higher facility pressures, therefore the ions do not strike with the maximum energy. It is not clear, however, why the mean impingement current was higher under these conditions than in the 1000 hour test. Further testing and modeling is required to understand these phenomena.

The original model calculated the impingement current for a given operating point based on the ratio of the impingement current and the beam current using data for mercury thrusters over a range of operating conditions. This ratio was characterized by a Beta distribution ranging from zero to 0.3 percent. Subsequent testing of the NSTAR thruster at low facility pressures has shown, however, that the true ratio is likely to be somewhat higher. The lowest value achieved at the full power point is approximately 0.3 percent, and these two tests indicate values closer to 0.5 percent.

The mass loss distribution is macroscopically nonuniform, decreasing with increasing grid radius. To first order the radial distribution of the charge exchange rate follows the radial beam current density distribution, which can be characterized by the flatness parameter. For lack of specific data on the

NSTAR thruster, this parameter was initially specified by a uniform distribution between 0.4 and 0.6, which are typical values for 30 cm optics [14]. Faraday probe data now available for the NSTAR thruster indicate that the flatness parameter is 0.41-0.42 at the full power point and decreases with engine power. In practice, the mass loss distribution off the grid is broadened relative to the beam current density profile by the radial motion of the charge exchange ions before they strike the grid. Destructive analyses of grids used in three long duration ion tests showed that the mass loss distribution was significantly broader than typical beam flatness parameters, an effect which may be aggravated under ground test conditions [12]. These grids have not been destructively analyzed, but the bridge and pit erosion depths as a function of radius can be compared with the beam current density distribution measured from FEMT2 in Figures (21) and (20). The pit depth radial distribution is similar to the beam profile out to about one half grid radius and then drops faster than the beam current density. This may be due to a broadening of the ion impingement current at larger radii, which the data in [12] suggest. If the pattern is wider at large radii, the wear depth may drop below the resolution of the measurement technique but still represent a flatter mass loss profile. In addition, for radii greater than about 11.6 cm the impingement current density is sufficiently low that net backscattered carbon deposition occurs. This is a facility effect which artificially suppresses the mass loss on the periphery. The probability of a charge exchange ion striking a facility carbon atom instead of a molybdenum atom is proportional to the surface coverage of carbon. Therefore, where the impingement current density is sufficiently high compared to the flux of backscattered material to maintain a low equilibrium carbon surface coverage the erosion rafts are essentially unaffected. This must occur at a relatively well-defined threshold current density, because the transition from net carbon deposition to the familiar pits and groove pattern is extremely sharp, occurring over about 5 mm at a radius of about 11.6 cm. The average bridge erosion depth appears to follow a more peaked distribution than the beam profile out to a radius of about 11 cm. At that point it also drops rapidly, probably for similar reasons. These indicators of the mass loss distribution suggest that it is more similar to the beam

current density distribution than previous data would indicate, although true mass loss distributions still need to be measured to verify this.

The mass loss is also distributed non-uniformly on a microscopic scale. The original model assumed that, the mass loss was confined locally to the pits and grooves pattern, which was characterized by a parameter referred to as the eroded area fraction. This is the fraction of the webbing area covered by the pits and grooves pattern. The eroded area fraction varies for different grid geometries and operating conditions [12] and the factors that control this parameter are not well understood, so it was originally treated parametrically in the probabilistic analysis [14]. These tests now provide some guidance in specifying this parameter and its variability. The groove width in the center of the grid used in this test was measured from photographs and used to calculate an eroded area fraction of 0.41-0.46. This is somewhat higher than the eroded area fraction of 0.37 estimated from photographs of the accelerator grid from the 2000 hour test. This is either representative of true variability or again a consequence of the different operating conditions.

Data from other grids suggests that the mass loss is not confined strictly to the pits and grooves pattern [12]. When the pits penetrate the grid a significant amount of material may be lost in undercutting on the upstream side. This test and the 2000 hour test suggest that significant mass loss may also occur on the walls of the apertures. New information gained from these tests has been used to refine the probabilistic analysis, as described in Ref. [16].

Screen Grid Erosion

Comparing the results of the two endurance tests demonstrates that the screen grid erosion rate is extraordinarily sensitive to the grid voltage relative to anode potential and the double ion fraction. When the screen grid is tied to cathode common it fixes this voltage difference at the discharge voltage. The discharge voltage and the double ion content can vary from the nominal values as the controllable engine parameters, such as beam current, power supply voltages and flowrates, are allowed to vary over specified limits. The sensitivity of these parameters to the allowable variations in the flight power processor and

feed system were measured in engine tests. A deterministic screen grid model that relates the maximum screen grid erosion to the double ion fraction, the grid potential and sputter yields has been adapted to a probabilistic framework with driver distributions specified by the sensitivity data [16]. This model yields results which agree well with erosion rates from the 2000 hour test and indicates that screen grid erosion is not a dominant failure mode for operation at the nominal conditions and allowable input parameter variability.

Flake Formation

This test yielded valuable information on the sources of sputtered material in the discharge chamber and the distribution of deposited mass. At these operating conditions the surface texturing in the discharge chamber appears to be adequate to contain flakes on anode surfaces. There are no measures so far to contain flakes from the screen grid however. The NSTAR program is relying on flake-clearing circuits with sufficient energy to vaporize grid-grid or grid-anode shorts, and operating experience so far suggests this may be sufficient. This potential failure mode has not yet been treated analytically, and because flake formation and grid shorting are inherently stochastic processes it will require probabilistic methods. Additional information on deposition rates and thin film flake formation mechanisms from testing are required [1].

Cathode Erosion

Cathode orifice plate and heater erosion is the least-understood of the wear processes observed in the 2000 hour test, in particular because the mechanism which produces energetic ions in the near cathode region is not known. Two mechanisms for ion acceleration to energies greater than the discharge potential have been proposed. Friedly and Wilbur suggested that the ions are accelerated from a potential hump close to the orifice [17]. Latham proposed that the current density in the orifice may be sufficiently high to create a self magnetic field that results in magneto-gasdynamical acceleration of the cathode plasma [18]. However, no attempt has yet been made to develop a quantitative model of the ion acceleration process

based on either of these mechanisms. The texturing of the cathode orifice plate and apparent shadowing in certain areas covered by the keeper suggests there is an ion source downstream of the keeper orifice. This demonstrates the effectiveness of the keeper as a physical barrier which protects the heater and parts of the cathode orifice plate. Fortunately the wear rate of the keeper orifice plate is relatively low; the problem was not simply transferred to the outermost surface. Experiments have been performed at Colorado State University which show that increasing tile neutral density in front of the cathode by injecting neutral gas near the cathode orifice reduces the erosion rate on surfaces downstream [19]. The keeper may serve to pressurize the region downstream of the cathode and therefore moderate the ion energies, which would explain the reduced erosion. However, the same effect might be caused by the higher cathode flow used in the 1000 hour test. Experiments have shown that increased flow through the cathode decreases the energy of ions in the cathode jet [19,18], but also increases the population of high energy ions. At this point it appears that the effects of the keeper and the increased flow rate compared to the 2000 hour test cannot be separated to identify specifically why the erosion was so dramatically reduced.

Appendix Determination of Flow Rate Correction

In this appendix the identification of xenon diffusion through the silicone rubber tubing as the culprit in the flow rate measurement error, the method used to correct the flow rates and a comparison with these measurements with published permeability data are presented. The indicated flow rate was observed to drop dramatically when a longer section of tubing was used to connect the bubble volumeter to the flow system. An experiment was then performed to confirm that diffusion through the tube walls was the cause of the suspected flow rate discrepancy. The mass loss rate through the tubing due to diffusion should be proportional to the exposed length of tubing. A series of calibrations performed with a range of tubing lengths, displayed in Fig. (22) shows exactly the expected behavior: longer sections of tubing result in progressively lower indicated flow rates.

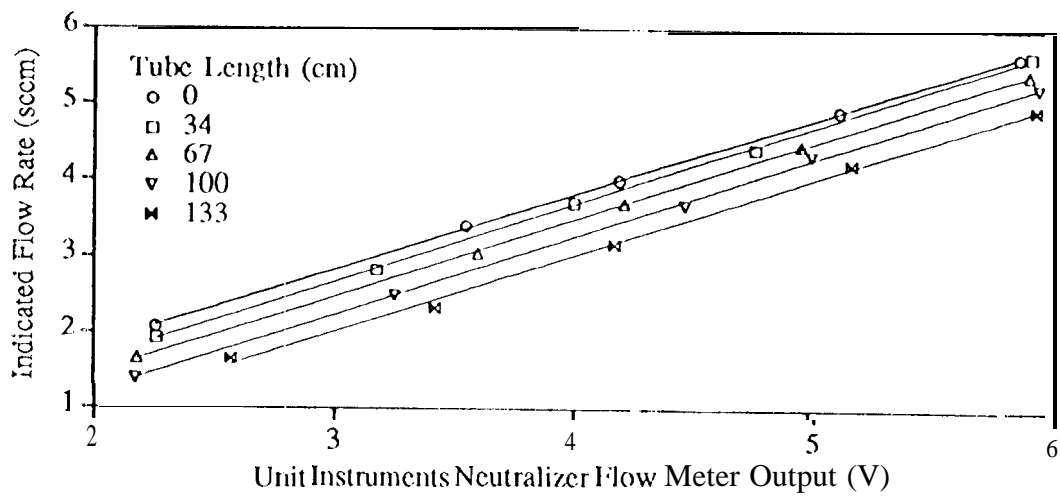


Figure 22: Indicated flow for varying lengths of silicone hose

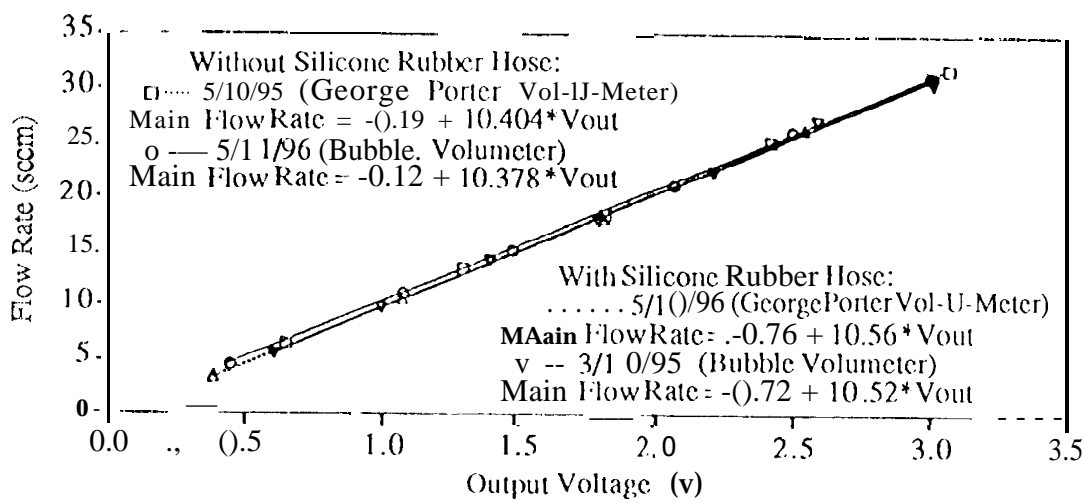


Figure 23: Comparisons of main flow meter calibrations.

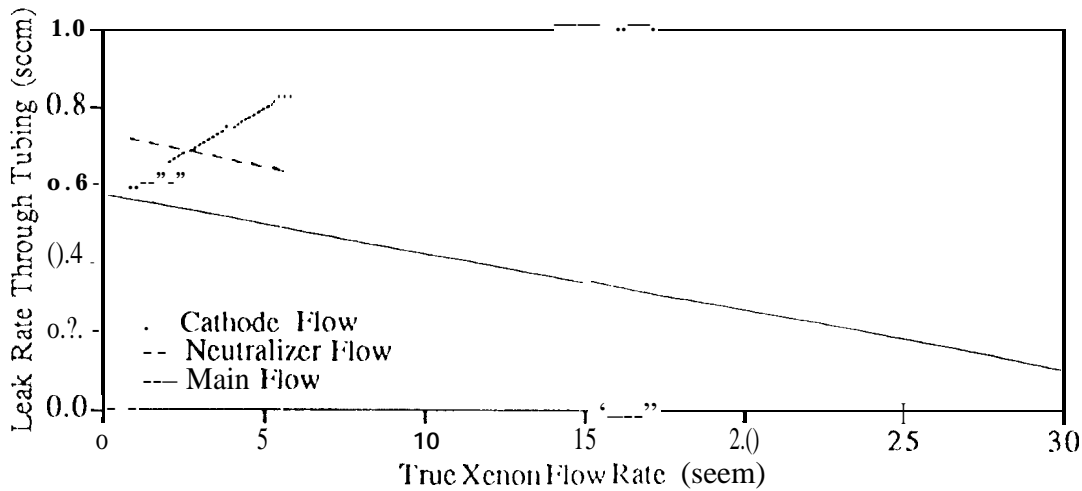


Figure 24: Xenon gas transfer rate as a function of total flow rate.

The individual flow meter calibrations were repeated with and without the 85 cm long section of hose used in all previous calibrations. The flow rates measured in these two calibrations were then subtracted to determine the xenon loss rate through the tubing wall. An example for the main flow is shown in Fig. (23). The bubble volumeter and the George K. Porter Vol-U-Meter calibrations of the main flow meter without the silicone rubber hose show excellent agreement, and an earlier bubble volumeter calibration performed with the hose was repeated to within 0.25 percent at the nominal main flow rate. The xenon loss rate through the tubing is plotted as a function of true flow for the three flow meters in Fig. (24). The leak rates associated with the neutralizer and cathode flow meter calibrations have opposite trends when plotted versus the true flow rate. However, they vary by only ± 0.1 seem, so this may just represent scatter in the measurements. The main flow meter calibration indicates an effective leak rate that agrees reasonably well with those measured by the other two flow meters at low flows but decreases with increasing true flow. It is not yet clear why this is so, but the repeatability of the calibrations suggests that it is a real effect. These data were used to correct the flow rates from the 1000 hour test for the xenon lost through the tubing during calibrations,

We subsequently discovered that silicone rubber tubing is one of the most permeable types of elastomer hose and that xenon has one of the highest permeabilities in silicone rubber. The mathematical treatment of gas diffusion through polymers is not unlike that of gas diffusion through liquids. The gas transfer rate is proportional to the concentration gradient and can be expressed in terms of Fick's Law, which can be rewritten in terms of a partial pressure gradient using Henry's law,

$$I^r = -P_B \nabla p \quad (1)$$

where the permeability constant P_B is the product of the diffusion coefficient and the solubility. This equation was solved for the case of a cylindrical geometry in which the only partial pressure gradient is assumed to be in the radial direction, and then integrated from the inner to the outer radius of the tube to obtain the flowrate per unit length of tubing. Using the measured permeability data from [20] the gas transfer rate through the wall of a silicone tube out into the ambient environment was calculated. These estimates assume a pure gas flowing in the tube so there is no mixing. The results are listed in Table (2) for nitrogen, argon and xenon. The supply pressure (partial pressure of the pure gas) is assumed to be 15 psi, the inner and outer tube radii are 0.32 cm and 0.64 cm, respectively. Because the ambient gas is air,

a partial pressure of 11.7 psi (78 percent) nitrogen is also assumed. (2). These results are intended to

Gas	$P_B \times 10^8$ (cc CII/ cm ² cm-Hg)	$F \times 10^4$ (seen./cm)	Gas Transfer (Rate) (Seem)
N ₂	1.67	1.6	0.014
Ar	4.27	18.0	0.153
Xe	19.2	81.0	0.689

Table 2: Calculated gas transfer rates in an 85 cm. long silicone hose using published permeability data.

be representative of silicone rubber in general. Differences in composite ion, due to the use of fillers to improve certain mechanical properties, are common and will alter the permeability values one measures with the products from different vendors. Nevertheless, the xenon gas transfer rate calculated from these data agrees remarkably well with the value determined from the flow calibrations at low flow rates. It also makes it clear why calibration comparisons with other standards using nitrogen and argon do not show this effect: their permeability in the tubing is much lower than that of xenon. Samples of the actual tubing used in the flow calibrations has been sent to several laboratories to measure the actual permeability to compare with these data.

Acknowledgements

The research described in this paper was conducted in part at the Jet Propulsion Laboratory, California Institute of Technology, and was sponsored by the National Aeronautics and Space Administration.

References

- [1] J.E. I'elk, N.R. Moore, J. It. Brophy, and D.H. Ebbeler. The Role of Analysis and Testing in the Service Life Assessment of Ion Engines. In *24th International Electric Propulsion Conference*, Moscow, Russia, 1995. IEPC-95-228.
- [2] M.J. Patterson. Low-Isp Derated Ion Thruster Operation. In *28th Joint Propulsion Conference*, Nashville, TN, 1992. AIAA-92-3203.
- [3] M.J. Patterson, T.W. Haag, and S.A. Hovan. Performance of the NASA 30 cm Ion Thruster. In *23rd International Electric Propulsion Conference*, Seattle, WA, 1993. AIAA-93-108 (Also NASA TM-1064226).
- [4] M.J. Patterson, V.K. Rawlin, J.S. Sovey, M.J. Kussmaul, and J. Parkes. 2.3 kW Ion Thruster Wear Test. In *31st Joint Propulsion Conference*, San Diego, CA, 1995. AIAA-95-2516.
- [5] J.L. Power and J.J. Iliznay. Solutions for Discharge Chamber Sputtering and Anode Deposit Spalling in Small Mercury Ion Thrusters. Technical Report TM X-71675, NASA Lewis Research Center, Cleveland, OH, 1975.
- [6] C.E. Garner, J.E. I'elk, J. It. Brophy, and L.C. Goodfellow. Methods for Cryopumping Xenon. In *32nd Joint Propulsion Conference*, Lake Buena Vista, FL, 1996. AIAA-96-3206.
- [7] C.E. Garner, J.R. Brophy, J.E. I'elk, and L.C. I'ess. A 5,730-Hr Cyclic Endurance Test of the SPT-100. In *24th International Electric Propulsion Conference*, Moscow, Russia, 1995. IEPC-95-179.
- [8] J.R. Brophy and C.E. Garner. A 5000 Hour Xenon Hollow Cathode Life Test. In *27th Joint Propulsion Conference*, Sacramento, CA, 1991. AIAA 91-2122.
- [9] J. It. Brophy, J.W. Barnett, J.M. Sankovic, and L.A. Barnhart. Performance of the Stationary Plasma Thruster: SI'1'-100. In *28th Joint Propulsion Conference*, Nashville, TN, 1992. AIAA 92-3833.
- [10] J. Mueller, May 1996. Personal communication.
- [11] J. It. Anderson and J. Fitzgerald. Experimental Investigation of Fullerene Propellant for Ion Propulsion. In *23rd International Electric Propulsion Conference*, Seattle, WA, 1993. AIAA-93-033.
- [12] J.E. I'elk, J.R. Brophy, and J.Wang. Spatial and Temporal Distribution of Ion Engine Accelerator Grid Erosion. In *31st Joint Propulsion Conference*, San Diego, CA, 1995. AIAA-95-2924.

- [13] J.R. Brophy, J.E. J'elk, and L.C. Pless. Test-to Failure of a Two Grid, 30-cm-dia. 1011 Accelerator System. In '23rd International Electric Propulsion Conference, Seattle, WA, 1993. AI AA-93-172.
- [14] J. E. J'elk, N. R. Moore, L. E. Newlin, J. R. Brophy, and D. H. Ebbeler. Probabilistic Analysis of Ion Engine Accelerator Grid Life. In 23rd International Electric Propulsion Conference, Seattle, WA, 1993. IEPC 93-176.
- [15] D. Rosenberg and G.K. Wehner. Sputtering Yields for Low Energy He⁺, Kr⁺ and Xe⁺ Ion Bombardment. *J. Appl. Phys.*, 33(5):1842-1845, 1962.
- [16] J.R. Brophy, J. E. Polk, and V.K. Rawlin. Ion Engine Service Life Validation by Analysis and Testing. in 32nd Joint Propulsion Conference, Lake Buena Vista, FL, 1996. AI AA-96-2715.
- [17] V. Friedly and T. Wilbur. High Current Hollow Cathode Phenomena. In 21st International Electric Propulsion Conference, Orlando, FL, 1990. AI AA-90-2587.
- [18] P.M. Latham, A.J Pearce, and R. A. Bond. Erosion Processes in the UK-25 Ion Thruster. In 22nd International Electric Propulsion Conference, Viareggio, Italy, 1991. AI AA-91-096.
- [19] T. Wilbur, Feb. 1996. Personal communication.
- [20] P. Kjeldsen. Evaluation of Gas Diffusion Through Plastic Materials Used in Experimental and Sampling Equipment. *Wat. Res.*, 27(1):121-131, 1993.